# Network pharmacology and *in vitro* experiments reveal the autophagy mechanism of Yanggan-Yishui granules in improving hypertensive renal injury

Pan Liu[1,2], Tairan Hu[3], Bing Gao[1], Ran Xia[1], Xiaohua Dai[3]*, Jing Wang[1]*

[1]Research Institute of Acupuncture and Meridian, Anhui University of Chinese Medicine, Yaohai District, Hefei, Anhui, China
[2]Department of Emergency or ICU, Anhui Provincial Hospital of Integrated Traditional and Western Medicine, Shushan District, Hefei, Anhui, China
[3]The First Affiliated Hospital of Anhui University of Traditional Chinese Medicine, Branch Center of the National Clinical Research Center for Cardiovascular Disease, Cardiovascular Institute of Anhui Academy of Chinese Medicine, Shushan District, Hefei, Anhui, China

*Corresponding authors:
Jing Wang
Research Institute of
Acupuncture and Meridian
Anhui University of
Chinese Medicine
Qianjiang Road
Yaohai District
Hefei 230012
Anhui, China
E-mail: wangjing2161@126.com

Xiaohua Dai
The First Affiliated
Hospital of Anhui
University of Traditional
Chinese Medicine
Branch Center of the
National Clinical Research
Center for Cardiovascular
Disease
Cardiovascular Institute of
Anhui Academy of
Chinese Medicine
117 Meishan Road
Shushan District
Hefei 230031
Anhui, China
mail: xin_d3980@163.com

## Abstract

**Introduction:** In China, Yanggan-Yishui granules (YGYSG) have been used to treat hypertensive renal damage (HRD) for over 20 years. Network pharmacology was used to determine whether YGYSG affects HRD via the autophagy pathway, which was verified using *in vitro* experiments.
**Material and methods:** Common targets of YGYSG, HRD, and the autophagy pathway were screened using network pharmacology, and effective compounds, core targets, and signaling pathways were identified. The affinity of the compounds for the core targets was evaluated using molecular docking simulations. Angiotensin II (Ang II) was used to generate an *in vitro* renal podocyte model using MPC-5 cells. Morphological changes in the autophagosomes were observed using transmission electron microscopy (TEM). The expression levels of autophagy-related and pathway proteins were detected using western blotting and reverse transcription quantitative real-time polymerase chain reaction (PCR).
**Results:** Network pharmacology and molecular docking analyses identified eight autophagy-related core targets and ten core components in the YGYSG treatment of HRD. These targets are mainly involved in the phosphoinositide 3-kinase (PI3K)/protein kinase B (AKT)/mammalian target of rapamycin (mTOR) signaling pathway and autophagy-related biological processes. *In vitro* experiments showed that Ang II-stimulated renal podocytes exhibited abnormal autophagy, and YGYSG protected renal podocytes from abnormal autophagy. In addition, YGYSG reversed abnormal autophagy and improved HRD by activating the PI3K/AKT/mTOR signaling pathway.
**Conclusions:** YGYSG may regulate abnormal autophagy in renal podocytes by activating the PI3K/AKT/mTOR signaling pathway and may play a role in improving HRD.

**Key words:** hypertensive renal impairment, network pharmacology, autophagy, PI3K/AKT/mTOR signaling pathway.

Pan Liu, Tairan Hu, Bing Gao, Ran Xia, Xiaohua Dai, Jing Wang

## Introduction

Hypertension is an independent risk factor for several clinical diseases and a controllable indicator of disease-related mortality [1]. Therefore, it has been listed as a global prevention target by the World Health Organization [2]. The number of people with hypertension worldwide is estimated to exceed 1.5 billion by 2025 [3]. Hypertensive renal damage (HRD) is a serious complication of hypertension. Long-term hypertension leads to renal vascular endothelial injury, glomerulosclerosis, and podocyte foot process effacement, resulting in renal fibrosis and increased risk of end-stage renal failure (ESRD) [4–6]. Therefore, it is important to effectively control HRD to delay its progression. Currently, angiotensin-converting enzyme inhibitors (ACEI), calcium channel blockers (CCBs), and diuretics are the main drugs used in the clinical treatment of hypertension [7, 8]. However, these drugs often have use-limiting side effects, including dry cough, lower limb edema, and enhanced sympathetic activity [9]. In addition, their effectiveness is limited. A data survey from Eastern European countries showed that after long-term antihypertensive treatment (including two or more antihypertensive drugs), only 30.8% of patients experienced effective hypertension control [10].

Owing to its long history and theoretical basis, traditional Chinese medicine (TCM) has played a significant role in the treatment of many diseases [11] including hypertension [12, 13]. Yang-gan-Yishui granules (YGYSG) were developed by Professor Zhou Yixuan, a renowned TCM practitioner in Anhui Province. These granules have been used clinically for over 20 years and have shown a remarkable effect on hypertensive kidney injury [14]. Clinical studies have demonstrated that YGYSG can improve patient symptoms, reduce the excretion of urinary microalbumin associated with early hypertensive renal damage, and enhance antihypertensive effects while reducing multiple cardiovascular risk factors [15, 16]. Existing research indicates that YGYSG exerts renal protective effects by inhibiting the Ang /TRPC6/NF- B pathway, thereby treating early hypertensive renal damage [17]. Additionally, YGYSG regulates the levels of TGF-β, PIK, and PKB in renal tissues, inhibiting early renal damage caused by hypertension [18]. YGYSG is composed of six Chinese herbs: *Salvia miltiorrhiza*, *Lycium lycii*, *Astragalus*, *Achyranthus oxideus*, *Gorgon euryale*, and *Cuscuta*. Studies have found that *S. miltiorrhiza* can regulate autophagy in podocytes through the phosphoinositide 3-kinase (PI3K)/protein kinase B (AKT)/mammalian target of rapamycin (mTOR) signaling pathway [19] and that *Astragalus* also exerts its effects by regulating inflammation and autophagy [20].

Autophagy is a biological process through which cells maintain the stability of their internal environment by degrading discarded organelles. Under physiological conditions, autophagy protects renal cells and participates in the regulation of kidney diseases [21, 22]. However, in long-term hypertension, excessive autophagy damages renal podocytes and blood vessels, resulting in podocyte death and accelerating the development of HRD [23, 24]. Therefore, identifying and regulating autophagy-related targets and signaling pathways in renal podocytes is key to effective disease therapy. Currently, activation of the renin-angiotensin-aldosterone system (RAAS) is considered the key pathogenesis of HRD. In the state of hypertension, the RAAS is activated and induces angiotensin II (Ang II) to increase blood pressure. Ang II expression is particularly evident in the kidneys; if its expression is abnormal, renal podocytes can easily be damaged [25, 26]. Autophagy is closely related to Ang II activity in the kidney, and it has been found that Ang II increase can upregulate the expression of autophagy in the kidney [27]. However, the underlying mechanism requires further investigation.

In this study, we identified possible targets and signaling pathways of YGYSG's modulation of the autophagy pathway through network pharmacological analysis. We then verified these findings using molecular docking technology and *in vitro* experiments. This provides evidence for the use of YGYSG in the treatment of HRD.

## Material and methods

### Screening of YGYSG, HRD, and autophagy targets

The drug composition of YGYSG was determined using the Traditional Chinese Medicine Systems Pharmacology Database (TCMSP) platform (https://lsp.nwu.edu.cn/tcmsp.php) [28], and screening criteria were set as oral availability (OB) ≥ 30% and drug-likeness (DL) ≥ 0.18; after obtaining the active ingredients, single drug targets were searched by drug MOL.ID number [29]. HRD and autophagy targets were obtained from GeneCards (https://www.genecards.org/) and OMIM (https://www.omim.org/) databases, respectively. The keywords 'hypertensive renal damage and autophagy' were entered into a disease database for retrieval, and the targets obtained from the two databases were combined. Finally, target names were converted using the UniProt database (https://www.uniprot.org). The Venny website (https://bioinfogp.cnb.csic.es/tools/venny/) provides access to the active ingredients in medicines, HRD, and common autophagy targets. These proteins can be used as key targets of YGYSG to treat HRD via the modulation of autophagy.

## Construction and analysis of the protein interaction network (PPI) in the treatment of HRD using YGYSG

The common protein-protein interaction (PPI) network of YGYSG, HRD, and the autophagy pathway was constructed using the STRING platform (https://string-db. org/) and the species was set as *Homo sapiens*. To ensure the reliability of the study, the confidence level was set to 0.9, and the other parameters were set to their default values. Cytoscape (version 3.9.0) software was used to import the TSV files and map the protein interaction network. A topological analysis was performed on the network. The degree value represents the size and color of the target. Component-target, core component-target-disease, and YGYSG core target pathway networks were constructed.

## Gene Ontology (GO) and Kyoto Encyclopedia of Genes and Genomes (KEGG) enrichment analysis

GO and KEGG analyses were performed using the Metascape (https://metascape.org/) database, with the screening criterion set at $p < 0.05$. The Microscopic Letter platform (http://www.bio-informatics.com.cn/) was used to generate visual images.

## Active ingredients-target molecular docking

For key component selection and molecular docking, the core targets of molecular docking small-molecule composition were identified using the TCMSP (https://old.tcmsp-e.com/) database and macromolecular proteins using the AlphaFold database (https://alphafold.ebi.ac=/). The protein crystal structure was dehydrated and hydrogenated using AutodockTools, and the receptor structure was prepared. OpenBabel and AutoDock were used to split the small-molecule library. Docking simulations were performed using Autodock software, and the results were imported into PyMOL for visualization.

## Drugs and reagents

YGYSG was provided by the Pharmacy Department of the First Affiliated Hospital of the Anhui University of Chinese Medicine. *Salvia miltiorrhiza*, *Lycium lycii*, *Astragalus*, *Achyranthus oxideus*, *Gorgon euryale*, and *Cuscuta* are Chinese herbal medicines. The granules were ground into an ultrafine powder and dissolved in a normal saline solution (PSS) to prepare a 100% stock solution (i.e., 1.0 g of powder per mL of PSS). The positive control drug benazepril (10 mg) was provided by the Pharmacy Department of the First Affiliated Hospital of Anhui University of Chinese Medicine. Ang II (5 mg) was purchased from Anhui Yingmai Biological Co. Ltd (Anhui, China). Fetal bovine serum (FBS) and HyClone High Sugar Dulbecco's Modified Eagle's Medium (DMEM) were purchased from Gibco (Grand Island, NY, USA). The Cell Counting Kit-8 (CCK-8) kit was purchased from Dojindo (Tokyo, Japan), and 0.25% trypsin-ethylenediaminetetraacetic acid (EDTA), penicillin-streptomycin solution, radioimmuno-precipitation assay (RIPA) lysate (09271919023), and anti-beclin-1 antibody (ab62472) were purchased from Abcam (Cambridge, UK). Anti-P62 (18420-1-AP), anti-LC3 (2775S), anti-Mtor (2972s), anti-Akt (4691S), and anti-PI3K (bsm-33219M) antibodies were purchased from Cell Signaling Technology (Danvers, MA, USA). The qPCR and gDNA remover RT Master Mix (RK20403) were obtained from AbClonal (Wuhan, China), and 3-methyladenine (3-MA) was provided by Anhui (China).

## Experimental animals

Thirty male Sprague Dawley (SD) rats weighing 200–250 g were obtained from the Experimental Center of the Anhui University of Chinese Medicine. All rats were provided with food and drinking water once a day and maintained at a constant temperature of 22 ±2°C and a humidity of 55–60%. This study was approved by the Experimental Animal Ethics Committee of Anhui University of Traditional Chinese Medicine (AHUCM-rats-2021135).

## Rat groups and preparation of YGYSG medicated serum

The rats were randomly divided into YGYS-high (YGYS-H), -medium (YGYS-M), and -low (YGYS-L) dose groups ($n \leq 10$), a positive control group ($n \leq 10$), and a blank group ($n \leq 10$). The YGYS-H, YGYS-M, and YGYS-L groups were administered daily doses of 0.64 g/ml, 0.32 g/ml, and 0.16 g/ml YGYS, respectively. Rats in the positive drug group were given 0.18 mg/ml of benazepril daily via oral gavage for 2 weeks. Animals in the control group received saline in the same manner and on the same schedule. One hour after the last gavage, all animals were anesthetized using an intraperitoneal injection of 3.5% pentobarbital sodium (10 ml/kg) after fasting for 24 h. Blood samples from the abdominal aorta were collected at room temperature for 2 h, and the complement was inactivated at 56°C for 30 min. Bacteria were removed by filtration twice with a 0.22 µm microporous membrane, and blood samples were then packaged, sealed, and stored in the refrigerator at –80°C for later use.

Pan Liu, Tairan Hu, Bing Gao, Ran Xia, Xiaohua Dai, Jing Wang

### Cell culture

MPC-5 renal podocytes were purchased from Yingmai Technology Co. Ltd. (Hefei, China). The cells were cultured in a complete medium consisting of high glucose DMEM, 10% FBS, and 1% penicillin-streptomycin in an incubator with 5% $CO_2$ at 37°C. When 70–80% of the cells were fused, 0.25% EDTA/trypsin solution was added to digest the cells. After digestion, DMEM containing 10% FBS was added to terminate digestion for subculturing.

### CCK-8 assay

MPC-5 cells were seeded into 96-well plates at a density of $1 \times 10^4$ cells/ml, with six wells per group. Upon reaching 70% confluence, cells were cultured for 12 h without serum to synchronize. Except for the control group, serum media containing YGYS-L, YGYS-M, and YGYS-H at concentrations of 5%, 10%, 15%, and 20% were added for 24 h. After incubation, 10 µl of CCK-8 solution was added to each well according to the manufacturer's instructions, followed by incubation for 1 h. The absorbance of each well was measured at 490 nm.

### Transmission electron microscopy (TEM)

Three groups of cells were selected for electron microscopy: blank, model, and optimal YGYSG concentration. MPC-5 cells were collected and placed in 1.5 ml of electron microscope fixative and stored in a refrigerator at 4°C for 6 h. The electron microscope-fixing solution was removed, 1.5 ml of PBS was added and the sample was allowed to soak for 1 h. Dehydration using ethanol was performed as follows at room temperature: 30% ethanol (1.5 ml, 10 min), 50% ethanol (1.5 ml, 10 min), 70% ethanol and saturated uranium dioxyacetate (1.5 ml, 3 h), 80% ethanol (1.5 ml, 10 min), 95% ethanol (1.5 ml, 15 min), and 100% ethanol (1.5 ml, 50 min); this was repeated twice. Finally, 1.5 ml propylene was added to the sample and allowed to stand for 30 min. Finally, the sample was sliced using an ultramicrotome to a thickness of 60–80 nm for observation.

### Western blotting

Total protein was extracted using RIPA lysis buffer. The proteins were quantified using the bicinchoninic acid method. Sodium dodecyl sulfate-polyacrylamide gel electrophoresis (SDS-PAGE) protein loading buffer 5X was added to the collected protein samples at a ratio of 1 : 4. A boiling water bath was used for 15 min to completely denature the proteins. After the sample cooled to room temperature, it was directly sampled into an SDS-PAGE gel sampling hole. We then added 5–10 µl to each well. Electrophoresis was carried out at 80 V for approximately 1 h. The membrane was then incubated with primary antibodies at 4°C overnight. The primary antibodies used were as follows: p62 (1 : 50 000), beclin-1 (1 : 1000), LC3 (1 : 1000), PI3K (1 : 1000), AKT (1 : 1000), mTOR (1 : 1000), and β-actin (1 : 1000).

### Reverse transcription quantitative polymerase chain reaction (RT-qPCR)

For RNA extraction, the cell precipitate was collected and 1 ml of TRIzol was added for cracking. After complete cracking, the cells were centrifuged at 12 000 rpm at 4°C for 15 min, and the supernatant was discarded. Pre-cooled 75% ethanol (1 ml) was added (anhydrous ethanol was diluted with diethyl pyrocarbonate-treated [DEPC] water). The solutions were centrifuged at 12 000 rpm at 4°C for 5 min, and the supernatant was discarded. RNA was dried at room temperature, precipitated with 20–50 µl of DEPC water, and stored at –80°C for later use. For the reaction, the mixture was gently mixed and centrifuged in a 0.2 ml EP tube. The samples were heated at 42°C for 2 min and immediately bathed in ice for 1 min. The EP tubes were then added to the PCR apparatus for the RT reaction. Lastly, the above reaction solution was removed and stored at –80°C for later use.

### Statistical analysis

Data were analyzed using GraphPad Prism (version 8.0.2) and SPSS (version 26.0) software. Data were expressed as mean ± standard deviation (mean ± SD). One-way analysis of variance was used for comparisons between groups, and the least significant difference (LSD) $t$-test was used for paired comparisons between groups. Statistical significance was set at $p < 0.05$.

## Results

### YGYSG core components act on targets of hypertensive kidney injury via the autophagy pathway

The workflow of the experiment is illustrated in Figure 1. A total of 129 effective components were obtained by retrieving the drug ingredients using the TCMSP database and setting oral bioavailability (OB) ≥ 30% and drug-likeness (DL) ≥ 0.18 as likeness conditions. Of these, 57 were *S. miltiorrhiza*, 34 were *Lycium lycii*, 15 were *Astragalus likeness*, 16 were *Achyranthes sinensis*, 2 were *Gorgon euryale*, and 10 were *Cuscuta* (Figure 2). By combining the GeneCards and OMIM database results, 7097 disease targets were obtained after removing duplicates, including 7074 and 96 targets from
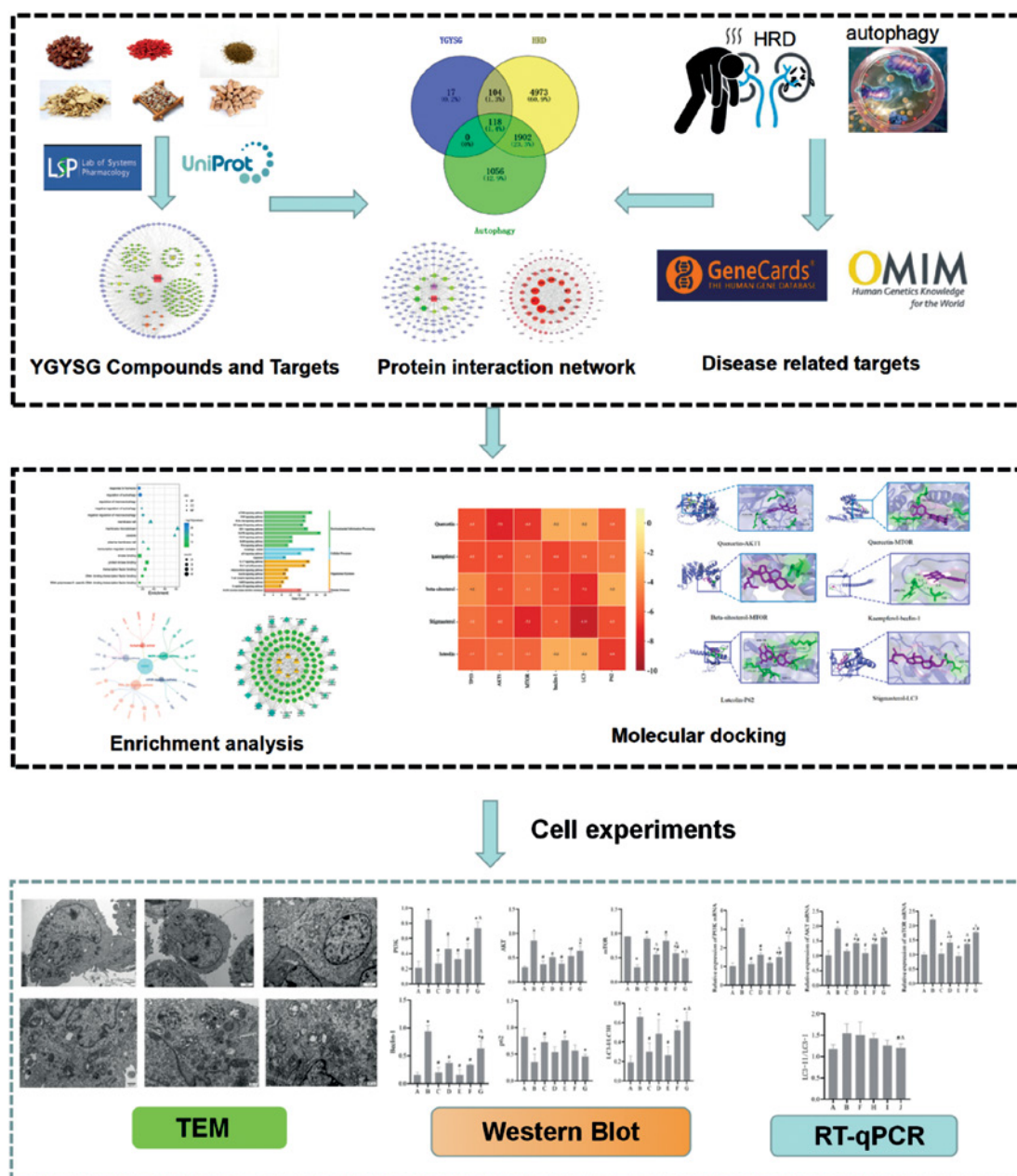
**Figure 1.** Workflow of the experiment

the GeneCards and OMIM databases, respectively. By searching for 'autophagy,' 3076 targets were obtained in the GeneCards database, 29 targets were obtained in the OMIM database, and 3076 autophagy genes were obtained after combining duplicate values. By screening the intersecting targets of YGYSG, autophagy, and HRD, 118 intersecting targets were identified (Figure 3 A). Ten core compounds of YGYSG used in the treatment of HRD were identified by degree screening (Table I): quercetin, kaempferol, beta-sitosterol, stigmasterol, luteolin, isorhamnetin, tanshinone IIa, 7-O-methylisomucronulatol, baicalein, and formononetin. By referring to target mapping in TCMSP, 118 protein names were translated into official names in

the UniProt database (Table II), and drug-composition-target and drug-composition-target-disease networks were constructed (Figure 3 B).

### Protein interaction analysis of YGYSG in the treatment of HRD through the autophagy pathway

Protein interactions were predicted using the STRING database (https://string-db.org/). A total of 118 common targets obtained from the Venn diagram were imported into the database. The PPI network was constructed using Cytoscape software with 108 nodes and 982 edges (Figures 4 A, B). Finally, core targets were screened through
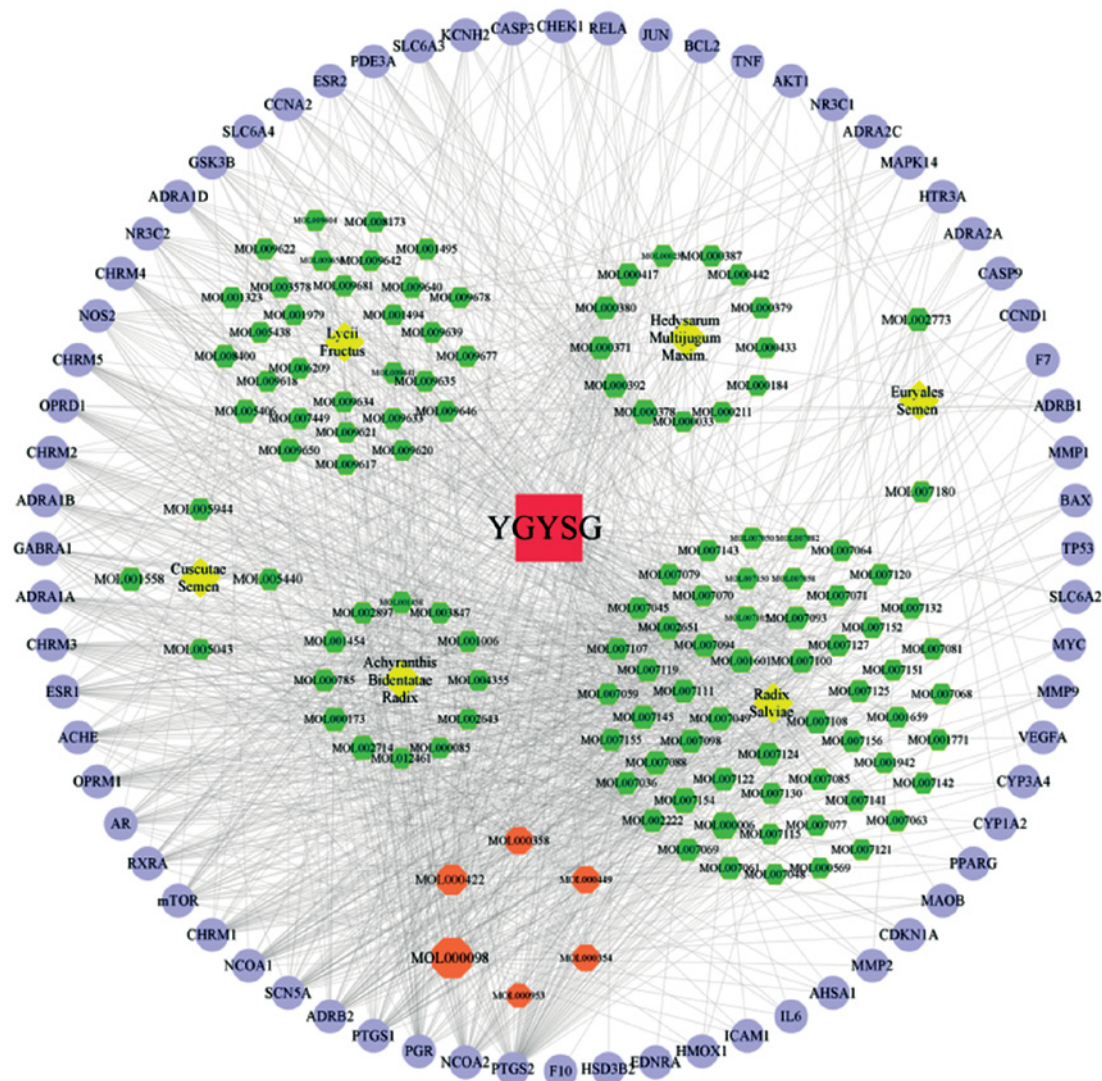
Pan Liu, Tairan Hu, Bing Gao, Ran Xia, Xiaohua Dai, Jing Wang



**Figure 2.** Construction of Yanggan-Yishui granules (YGYSG) component target network; the blue circle, green hexagon, pink hexagon, yellow diamond, and dark red squares represent drug target, drug component, drug common component, and traditional Chinese medicine, and YGYSG, respectively

the cytoHubba plugin; betweenness (BC), closeness (CC), and degree (DC) medians were used as screening criteria (Figure 4 C). The key core targets identified were as follows: cellular tumor antigen p53 (TP53), RAC-alpha serine/threonine-protein kinase (AKT1), signal transducer and activator of transcription 3 (STAT3), transcription factor AP-1 (JUN), caspase-3 (CASP3), tumor necrosis factor (TNF), serine/threonine-protein kinase mTOR (MTOR), and epidermal growth factor receptor (MAPK1 mitogen-activated protein kinase 1, EGFR) (Figure 4 D).

### Enrichment analysis of YGYSG treatment of HRD through the autophagy pathway

For an enrichment analysis using the Metascape website, 118 intersection targets were imported. The results showed that 1747 targets

related to biological processes (BP), 90 targets related to cell components (CC), and 141 targets related to molecular functions (MF) were selected (Figure 5 A). A total of 190 KEGG samples were obtained, most of which were primarily involved in the biological processes of hormones, nitrogen compounds, autophagy, kinase binding, protein kinase binding, and transcription factor binding (Figure 5 B). KEGG analysis results mainly involved the PI3K/AKT, mTOR, HIF-1, IL-17, MAPK, VEGF, autophagy-animal, T cell receptor, and NF-kappaB signaling pathways, and a drug-target-pathway network was simultaneously constructed (Figure 5 C). We further analyzed the enrichment pathways of the eight core targets (Figure 6 A). The results showed that the targets were mainly enriched in the PI3K/AKT, autophagy-animal, mTOR, MAPK, and TNF signaling pathways, among which
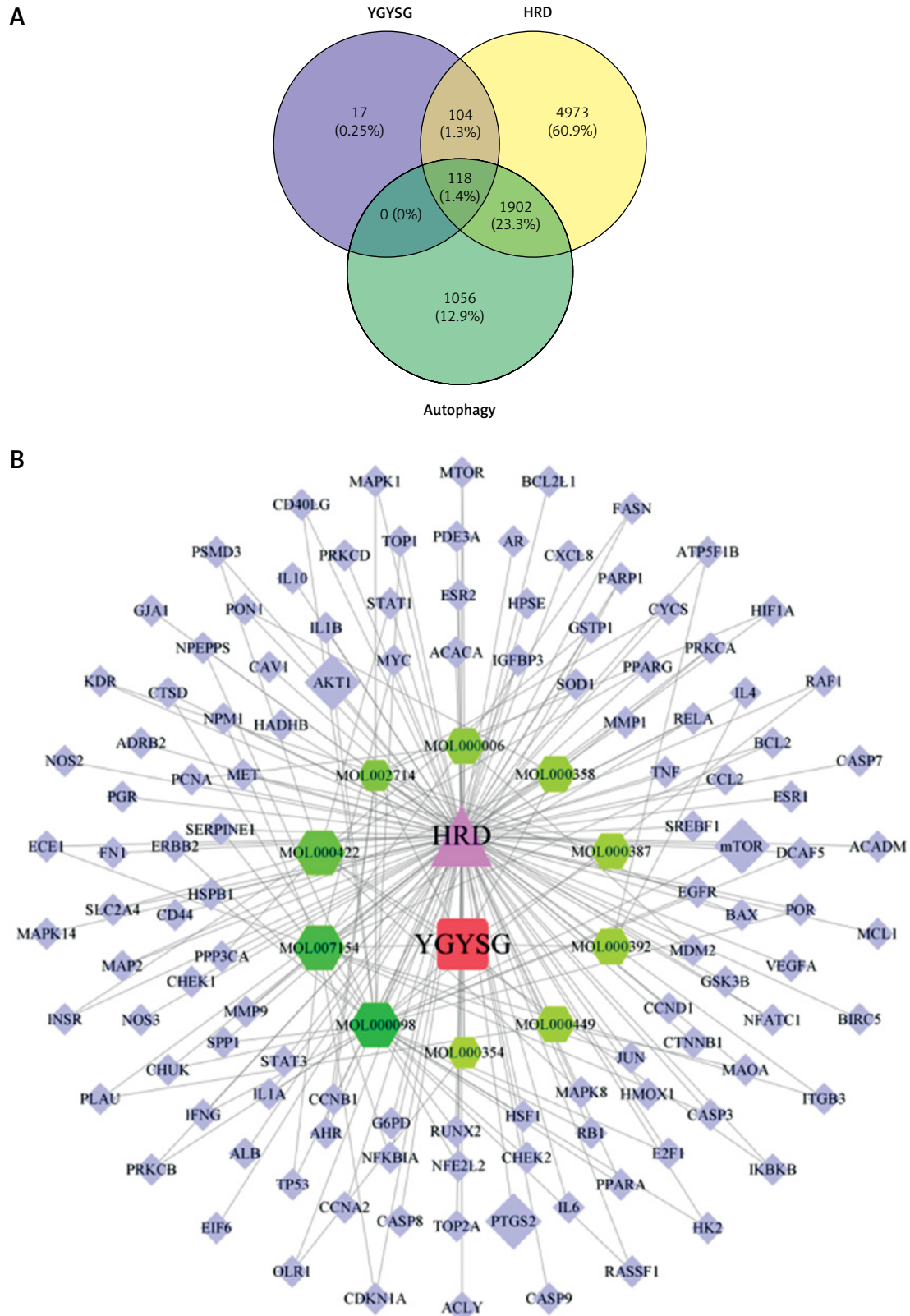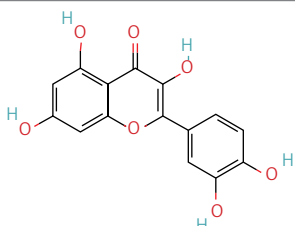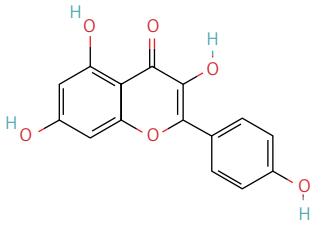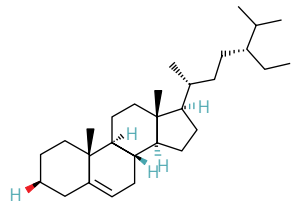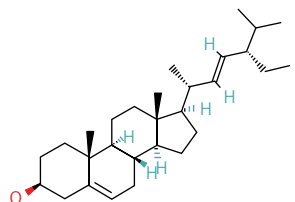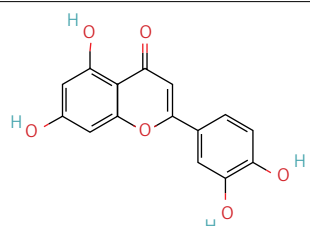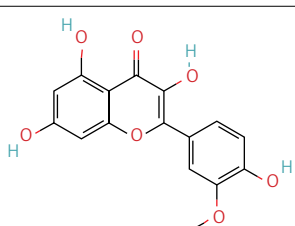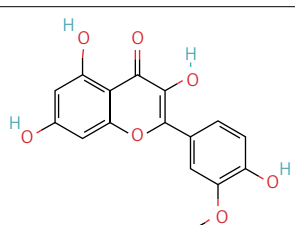
**Figure 3. A** – Wayne diagram of the intersection of Yanggan-Yishui granules (YGYSG), hypertensive renal damage (HRD), and autophagy; **B** – YGYSG core component target disease network construction; the blue diamond, green hexagon, red square, and purple triangle represent intersection targets, core components, drugs, and diseases, respectively

**Table I.** Ten core compounds of YGYSG in HRD treatment. YGYSG: Yanggan-Yishui granules; HRD: hypertensive renal damage

| MOL ID | Active ingredient | Molecular structure | Molecular weight | OB% | DL | Degree |
|--------|-------------------|---------------------|------------------|------|------|--------|
| MOL000098 | Quercetin | | 302.23 | 46.43 | 0.28 | 516 |
| MOL000422 | Kaempferol | | 286.24 | 41.88 | 0.24 | 153 |
| MOL000358 | Beta-sitosterol | | 414.7 | 36.91 | 0.75 | 84 |
| MOL000449 | Stigmasterol | | 412.7 | 43.83 | 0.76 | 52 |
| MOL000006 | Luteolin | | 286.24 | 36.16 | 0.25 | 50 |
| MOL000354 | Isorhamnetin | | 316.26 | 49.60 | 0.31 | 46 |
| MOL007154 | Tanshinone iia | | 294.3 | 49.89 | 0.40 | 36 |

| MOL000378 | 7-O-methylisomu-cronulatol | | 316.3 | 74.69 | 0.30 | 33 |
|---|---|---|---|---|---|---|
| MOL002714 | Baicalein | | 270.24 | 33.52 | 0.21 | 31 |
| MOL000392 | Formononetin | | 268.26 | 66.39 | 0.21 | 29 |
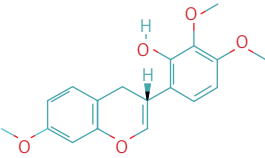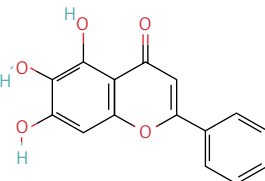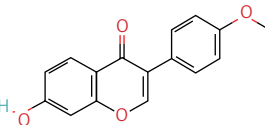
**Table II.** Target information of HRD treated by YGYSG through the autophagy pathway

| No. | Gene name | Protein name | Degree |
|---|---|---|---|
| 1 | NOS2 | Nitric oxide synthase, inducible | 63 |
| 2 | PTGS2 | Prostaglandin G/H synthase 2 | 62 |
| 3 | ESR1 | Estrogen receptor | 53 |
| 4 | MTOR | Serine/threonine-protein kinase mTOR | 52 |
| 5 | ADRB2 | Beta-2 adrenergic receptor | 47 |
| 6 | TP53 | Cellular tumor antigen p53 | 44 |
| 7 | RELA | Transcription factor p65 | 41 |
| 8 | NPM1 | Nucleophosmin | 40 |
| 9 | NFKBIA | NF-kappa-B inhibitor alpha | 39 |
| 10 | MYC | Myc proto-oncogene protein | 38 |
| 11 | MMP9 | Matrix metalloproteinase-9 | 37 |
| 12 | JUN | Transcription factor AP-1 | 36 |
| 13 | ITGB3 | Integrin beta-3 | 35 |
| 14 | FASN | Fatty acid synthase | 32 |
| 15 | ECE1 | Endothelin-converting enzyme 1 | 32 |
| 16 | CDKN1A | Cyclin-dependent kinase inhibitor 1 | 31 |
| 17 | CASP3 | Caspase-3 | 30 |
| 18 | BCL2 | Apoptosis regulator Bcl-2 | 30 |
| 19 | PDE3A | cGMP-inhibited 3 ,5 -cyclic phosphodiesterase A | 29 |
| 20 | PGR | Progesterone receptor | 29 |
| 21 | CCNA2 | Cyclin-A2 | 29 |
| 22 | GSK3B | Glycogen synthase kinase-3 beta | 26 |
| 23 | ESR2 | Estrogen receptor beta | 26 |
| 24 | CHEK1 | Serine/threonine-protein kinase Chk1 | 26 |
| 25 | TNF | Tumor necrosis factor | 25 |
| 26 | STAT3 | Signal transducer and activator of transcription 3 | 25 |
| 27 | CCND1 | G1/S-specific cyclin-D1 | 25 |
| 28 | BIRC5 | Baculoviral IAP repeat-containing protein 5 | 24 |
| 29 | BCL2L1 | Bcl-2-like protein 1 | 24 |
| 30 | MAPK14 | Mitogen-activated protein kinase 14 | 24 |
| 31 | TOP2A | DNA topoisomerase 2-alpha | 24 |

**Table II.** Cont.

| No. | Gene name | Protein name | Degree |
|-----|-----------|--------------|--------|
| 32 | VEGFA | Vascular endothelial growth factor A | 24 |
| 33 | TOP1 | DNA topoisomerase 1 | 23 |
| 34 | SLC2A4 | Solute carrier family 2, facilitated glucose transporter member 4 | 23 |
| 35 | RB1 | Retinoblastoma-associated protein | 22 |
| 36 | PPARG | Peroxisome proliferator-activated receptor gamma | 22 |
| 37 | PCNA | Proliferating cell nuclear antigen | 21 |
| 38 | MMP1 | Interstitial collagenase | 21 |
| 39 | MET | Hepatocyte growth factor receptor | 20 |
| 40 | MDM2 | E3 ubiquitin-protein ligase Mdm2 | 19 |
| 41 | MCL1 | Induced myeloid leukemia cell differentiation protein Mcl-1 | 19 |
| 42 | MAPK1 | Mitogen-activated protein kinase 1 | 19 |
| 43 | INSR | Insulin receptor | 19 |
| 44 | IL6 | Interleukin-6 | 18 |
| 45 | IL4 | Interleukin-4 | 18 |
| 46 | IL10 | Interleukin-10 | 18 |
| 47 | IFNG | Interferon gamma | 17 |
| 48 | HMOX1 | Heme oxygenase 1 | 17 |
| 49 | GSTP1 | Glutathione S-transferase P | 17 |
| 50 | ERBB2 | Receptor tyrosine-protein kinase erbB-2 | 16 |
| 51 | EGFR | Epidermal growth factor receptor | 16 |
| 52 | CD40LG | CD40 ligand | 15 |
| 53 | CCNB1 | G2/mitotic-specific cyclin-B1 | 15 |
| 54 | CASP9 | Caspase-9 | 15 |
| 55 | CASP7 | Caspase-7 | 15 |
| 56 | AKT1 | RAC-alpha serine/threonine-protein kinase | 15 |
| 57 | PLAU | Urokinase-type plasminogen activator | 14 |
| 58 | MAOA | Amine oxidase [flavin-containing] A | 14 |
| 59 | PRKCA | Protein kinase C alpha type | 14 |
| 60 | PON1 | Serum paraoxonase/arylesterase 1 | 14 |
| 61 | MAP2 | Microtubule-associated protein 2 | 14 |
| 62 | CASP8 | Caspase-8 | 13 |
| 63 | BAX | Apoptosis regulator BAX | 13 |
| 64 | STAT1 | Signal transducer and activator of transcription 1-alpha/beta | 13 |
| 65 | SPP1 | Osteopontin | 12 |
| 66 | SOD1 | Superoxide dismutase [Cu-Zn] | 12 |
| 67 | SERPINE1 | Plasminogen activator inhibitor 1 | 12 |
| 68 | RUNX2 | Runt-related transcription factor 2 | 12 |
| 69 | RASSF1 | Ras association domain-containing protein 1 | 12 |
| 70 | RAF1 | RAF proto-oncogene serine/threonine-protein kinase | 12 |
| 71 | PSMD3 | 26S proteasome non-ATPase regulatory subunit 3 | 12 |
| 72 | PRKCB | Protein kinase C beta type | 11 |
| 73 | PPARA | Peroxisome proliferator-activated receptor alpha | 11 |
| 74 | POR | NADPH-cytochrome P450 reductase | 11 |
| 75 | PARP1 | Poly [ADP-ribose] polymerase 1 | 11 |
| 76 | NPEPPS | Puromycin-sensitive aminopeptidase | 10 |
| 77 | NOS3 | Nitric oxide synthase, endothelial | 10 |

**Table II.** Cont.

| No. | Gene name | Protein name | Degree |
|-----|-----------|--------------|--------|
| 78 | NFE2L2 | Nuclear factor erythroid 2-related factor 2 | 10 |
| 79 | IRF1 | Interferon regulatory factor 1 | 9 |
| 80 | IL1B | Interleukin-1 beta | 9 |
| 81 | IL1A | Interleukin-1 alpha | 9 |
| 82 | IGFBP3 | Insulin-like growth factor-binding protein 3 | 9 |
| 83 | HSPB1 | Heat shock protein beta-1 | 8 |
| 84 | HSF1 | Heat shock factor protein 1 | 8 |
| 85 | HK2 | Hexokinase-2 | 8 |
| 86 | HIF1A | Hypoxia-inducible factor 1-alpha | 7 |
| 87 | GJA1 | Gap junction alpha-1 protein | 7 |
| 88 | EIF6 | Eukaryotic translation initiation factor 6 | 6 |
| 89 | E2F1 | Transcription factor E2F1 | 6 |
| 90 | DCAF5 | DDB1- and CUL4-associated factor 5 | 6 |
| 91 | CXCL8 | Interleukin-8 | 5 |
| 92 | CTSD | Cathepsin D | 5 |
| 93 | CHUK | Inhibitor of nuclear factor kappa-B kinase subunit alpha | 5 |
| 94 | CHEK2 | Serine/threonine-protein kinase Chk2 | 5 |
| 95 | CCL2 | C-C motif chemokine 2 | 4 |
| 96 | CAV1 | Caveolin-1 | 4 |
| 97 | AHR | Aryl hydrocarbon receptor | 4 |
| 98 | ACACA | Acetyl-CoA carboxylase 1 | 4 |
| 99 | PPP3CA | Serine/threonine-protein phosphatase 2B catalytic subunit alpha isoform | 4 |
| 100 | MAPK8 | Mitogen-activated protein kinase 8 | 4 |
| 101 | IKBKB | Inhibitor of nuclear factor kappa-B kinase subunit beta | 4 |
| 102 | ATP5F1B | ATP synthase subunit beta, mitochondrial | 3 |
| 103 | KDR | Vascular endothelial growth factor receptor 2 | 3 |
| 104 | OLR1 | Oxidized low-density lipoprotein receptor 1 | 2 |
| 105 | NFATC1 | Nuclear factor of activated T-cells, cytoplasmic 1 | 2 |
| 106 | CYCS | Cytochrome c | 2 |
| 107 | PRKCD | Protein kinase C delta type | 2 |
| 108 | FN1 | Fibronectin | 1 |
| 109 | ALB | Serum albumin | 1 |
| 110 | CTNNB1 | Catenin beta-1 | 1 |
| 111 | HPSE | Heparanase | 1 |
| 112 | CD44 | CD44 antigen | 1 |
| 113 | SREBF1 | Sterol regulatory element-binding protein 1 | 1 |
| 114 | HADHB | Trifunctional enzyme subunit beta, mitochondrial | 1 |
| 115 | G6PD | Glucose-6-phosphate 1-dehydrogenase | 1 |
| 116 | ACLY | ATP-citrate synthase | 1 |
| 117 | ACADM | Medium-chain specific acyl-CoA dehydrogenase, mitochondrial | 1 |
| 118 | AR | Androgen receptor | 1 |

*YGYSG – Yanggan-Yishui granules, HRD – hypertensive renal damage.*

Pan Liu, Tairan Hu, Bing Gao, Ran Xia, Xiaohua Dai, Jing Wang
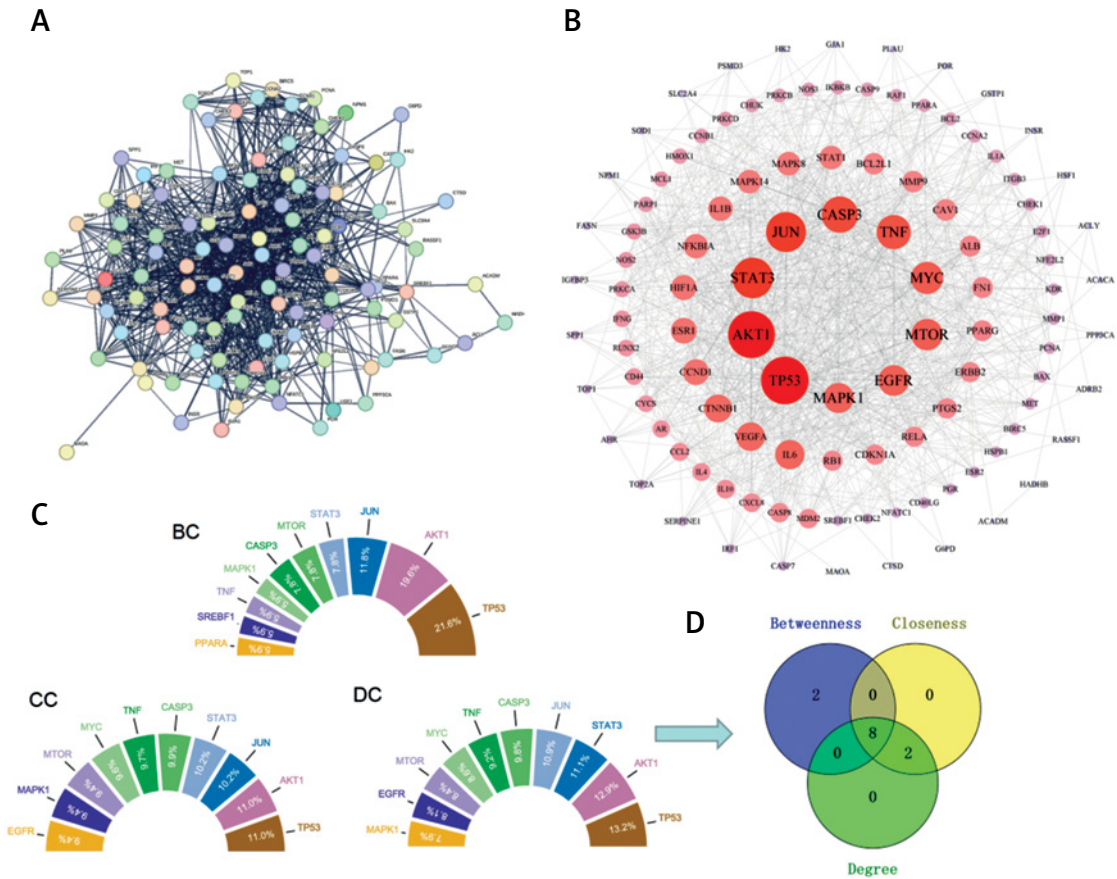
A



B



C



D



**Figure 4. A** – STRING PPI network obtained from the database; the highest protein interaction score was set as 0.9. **B** – In the PPI network constructed by Cytoscape software, the size of the circle and the shade of red were positively correlated with the degree value. **C** – According to the cytoHubba plugin, BC ≥ 0.011 (median), CC ≥ 0.495 (median), and DC ≥ 32 (median) should be screened. The sector area of each target in the figure was positively correlated with the percentage. **D** – Wayne diagram of intersection targets of BC, CC, and DC modules

A
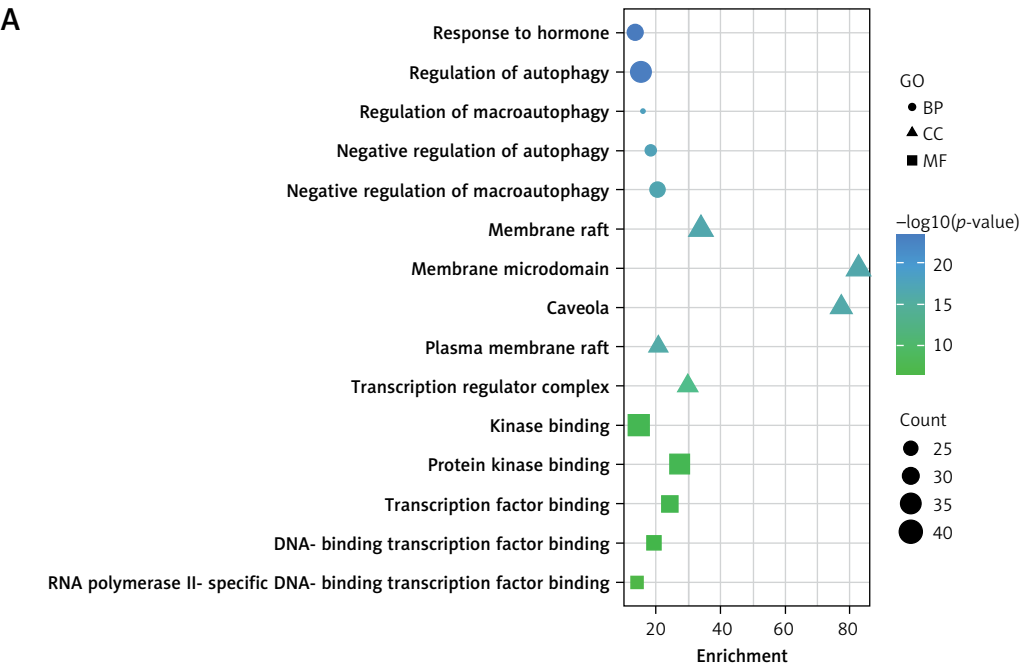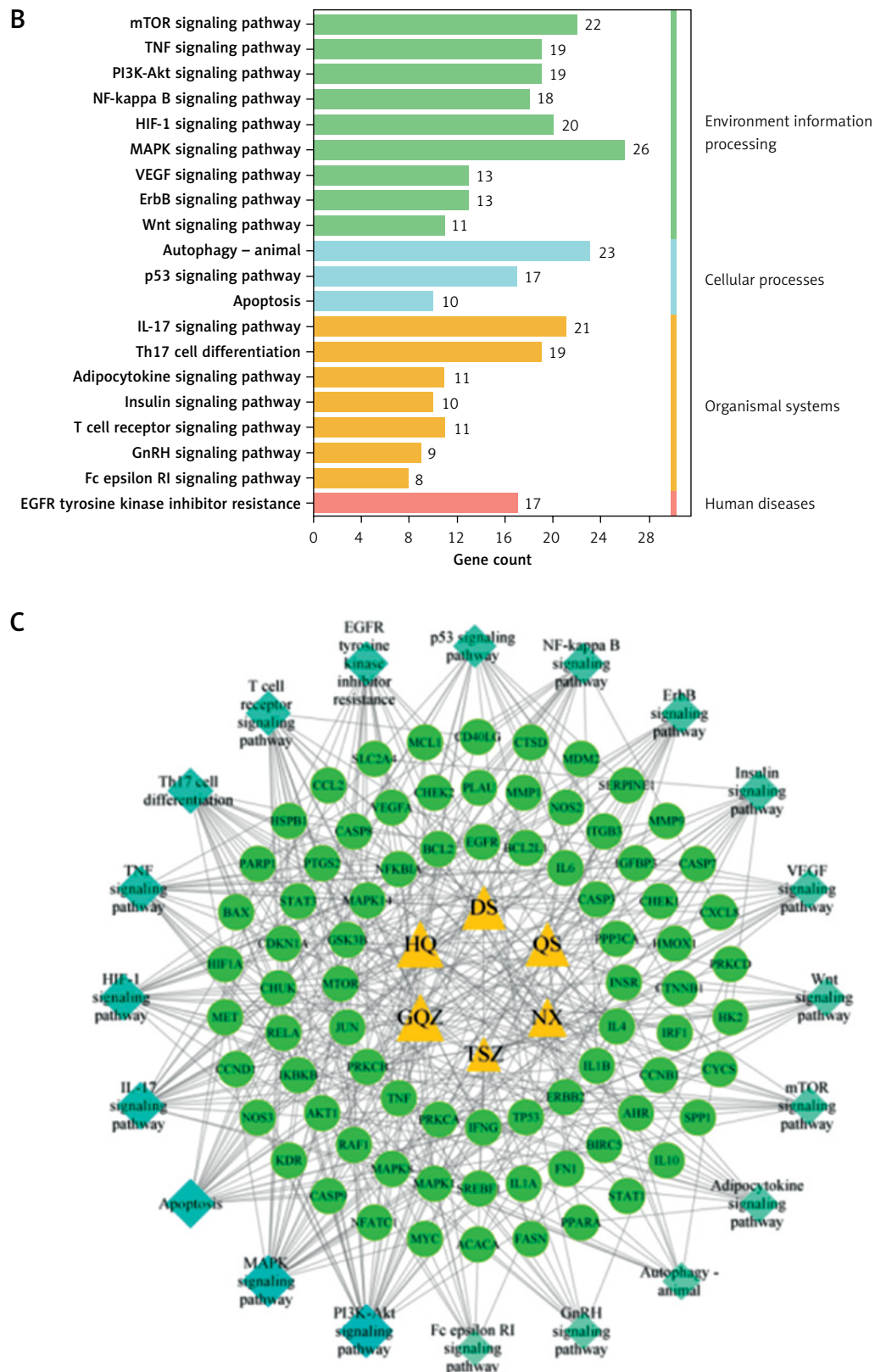


**Figure 5. A** – Gene Ontology (GO) analysis

**Figure 5.** Cont. **B** – Kyoto Encyclopedia of Genes and Genomes (KEGG) analysis; **C** – Drug target-pathway network

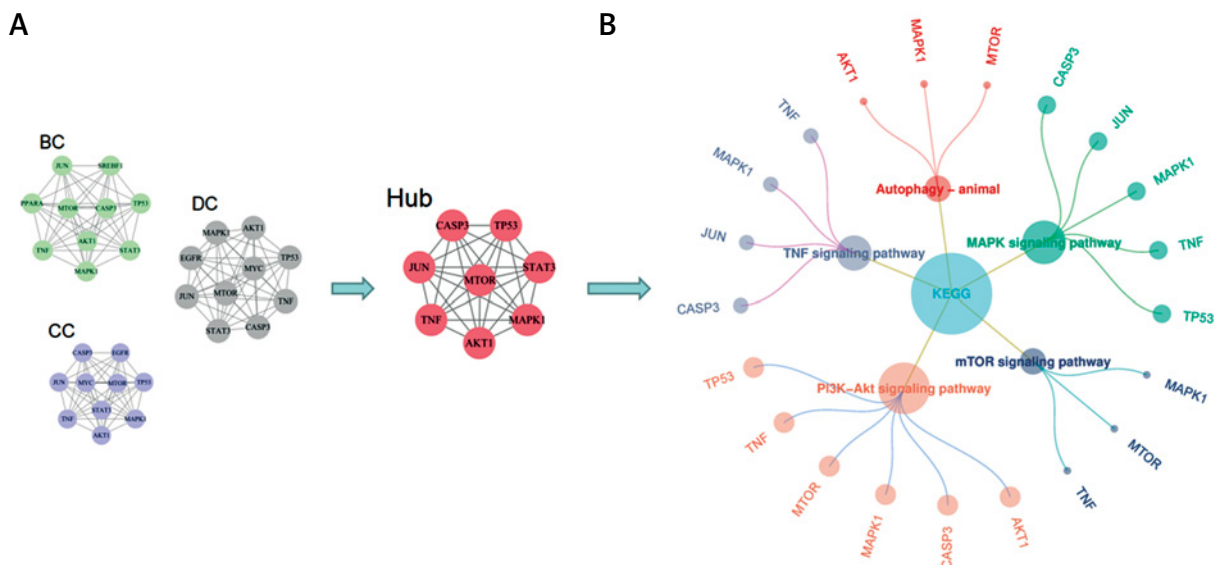Pan Liu, Tairan Hu, Bing Gao, Ran Xia, Xiaohua Dai, Jing Wang

**A**



**B**

**Figure 6. A** – Three topology modules selected by the cytoHubba plugin (2.1.2). Betweenness (BC), closeness (CC), and degree (DC) protein interaction networks were constructed by Cytoscape software, and core interaction networks were constructed according to the eight core targets. **B** – Significant signal pathway obtained from core target enrichment. At the same time, a three-layer circular network diagram was constructed. Different colors represent different signal pathways and enrichment targets, respectively, and node size represents the number of enriched targets

the PI3K/AKT signaling pathway was the most significant (Figure 6 B). Therefore, the PI3K/AKT signaling pathway was selected for further experiments.

### Molecular docking

Molecular docking simulations demonstrated the affinity of core components for core targets. The top five core components of the molecular docking small-molecule selection were quercetin, kaempferol, beta-sitosterol, stigmasterol, and luteolin, whereas the core targets TP53, AKT1, mTOR, and autophagy-related proteins beclin-1, LC3, and P62 ranked at the top in the macromolecular selection topology (Figure 7 A). Quercetin, kaemp-

ferol, beta-sitosterol, stigmasterol, and luteolin exhibited good binding energies for TP53, AKT1, mTOR, beclin-1, LC3, and P62. The six groups of visual displays with the best docking results were selected (Figure 7 B).

### Optimal serum concentration of YGYSG

We studied the effect of different concentrations of YGYSG-medicated serum on the viability of MPC-5 cells. Cells were treated with low, medium, and high doses of YGYS-medicated serum at concentrations of 5, 10, 15, and 20% for 12, 24, and 48 h, and a CCK-8 assay was performed to calculate cell viability. Default cell viability in the control group was 100%. In the YGYS-L group,
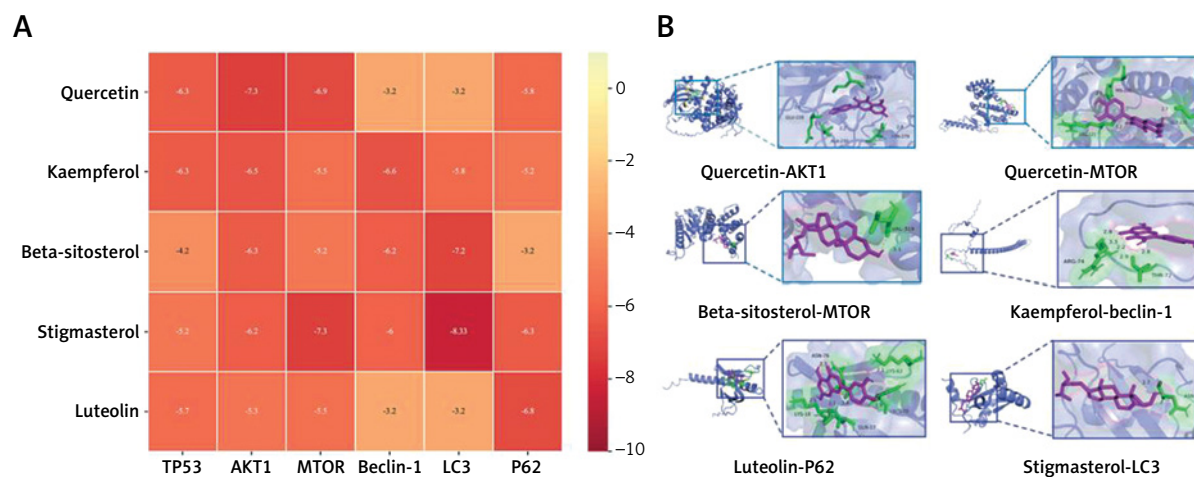
**A**



**B**

**Figure 7. A** – Heat map of bonding energy; **B** – Docking diagram of core component targets

cell viability at 5% concentration after 24 h was significantly higher than that in the control group ($p < 0.01$, Figure 8 A). In YGYS-M, the cell viability at 5% YGYS drug-containing serum for 12, 24, and 48 h, 10% YGYS drug-containing serum for 24 and 48 h, and 15% YGYS drug-containing serum for 24 h was significantly higher than that of the control group ($p < 0.01$, Figure 8 B). In addition, compared to the 20% YGYS drug-containing serum, the 5% YGYS drug-containing serum showed significantly higher cell viability after 24 h of treatment ($p < 0.05$, Figure 8 B). In the YGYS-H group, compared to the control group, the 15% YGYSG drug-containing serum showed significantly higher cell viability after 48 h of treatment ($p < 0.01$, Figure 8 C). Therefore, MPC-5 cells were treated with 5% concentration of YGYS-M for 24 h for TEM. Western blotting and RT-qPCR experiments employed 5% YGYS-L treatment of MPC-5 cells for 24 h, 5% YGYS-M treatment of MPC-5 cells for 24 h, and 15% YGYS-H treatment of MPC-5 cells for 48 h (Table III).

### YGYSG medicated serum inhibited autophagy of MPC-5 cells

We studied the presence of autophagic vacu-

oles using TEM. TEM observations showed that autophagosomes in the normal group had a normal morphology and organelle structure. Ang II-stimulated podocytes showed over-expanded autophagosomes, the number of which increased greatly, and the structure of the organelles was destroyed. The organelles of YGYSG-treated cells appeared intact, the autophagosomes were smaller in shape and significantly reduced in number, and the double-layer membrane structure of the autophagosomes was complete (Figure 9). These morphological changes indicated that YGYSG inhibited autophagy in renal podocytes.

### YGYSG inhibits autophagy of MPC-5 cells through the PI3K/AKT/mTOR signaling pathway

To explore the precise role of YGYSG-medicated serum in Ang II-induced autophagy of MPC-5 cells, western blotting and RT-qPCR were employed to measure the levels of PI3K/AKT/mTOR signaling pathway and autophagy-related markers. The results showed that, compared with the control group, the protein expression of PI3K, AKT, and beclin-1 in the model and YGYS-L groups was elevated ($p < 0.05$, Figures 10, 11) and the
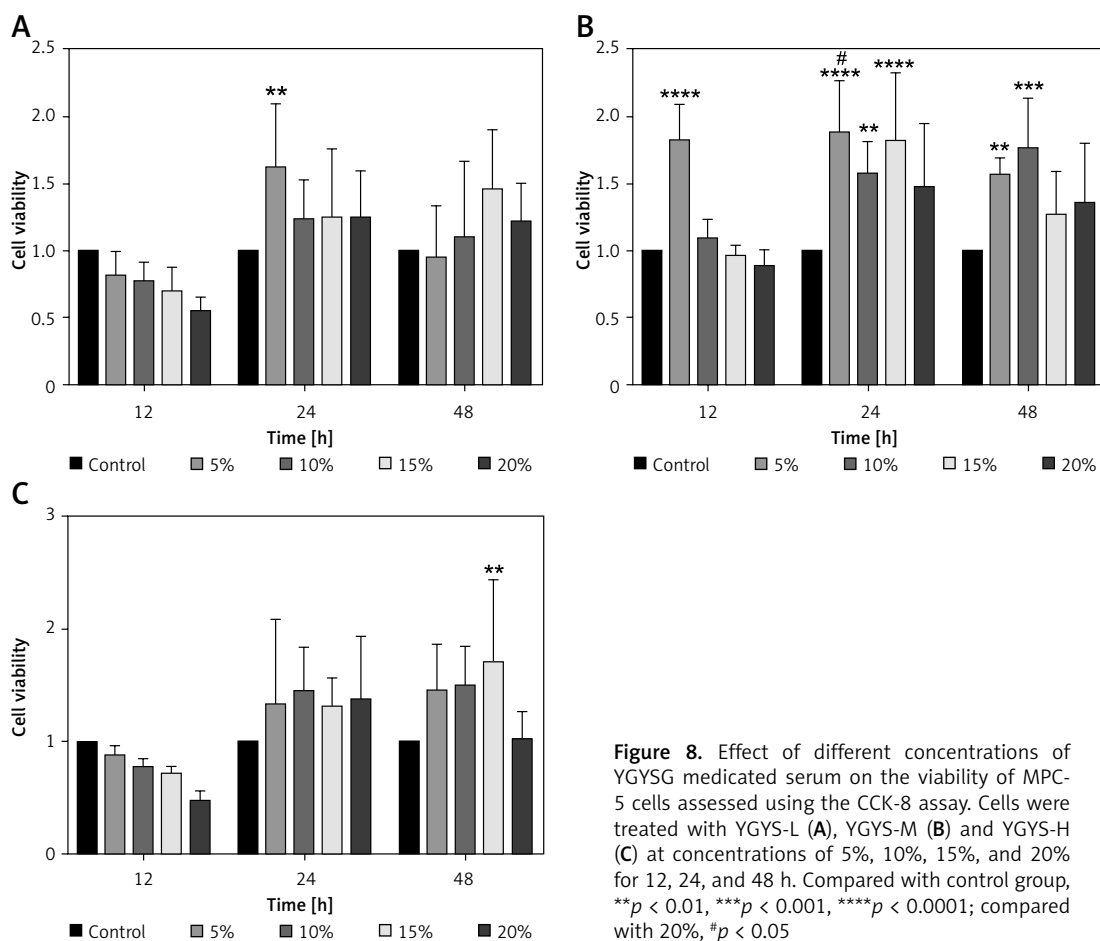


**Figure 8.** Effect of different concentrations of YGYSG medicated serum on the viability of MPC-5 cells assessed using the CCK-8 assay. Cells were treated with YGYS-L (**A**), YGYS-M (**B**) and YGYS-H (**C**) at concentrations of 5%, 10%, 15%, and 20% for 12, 24, and 48 h. Compared with control group, **$p < 0.01$, ***$p < 0.001$, ****$p < 0.0001$; compared with 20%, #$p < 0.05$

**Table III.** Effects of different concentrations of drug-containing serum at different time points on the activity of MPC-5 cells (± S)

| Groups | Serum concentration | Time | | |
|---|---|---|---|---|
| | | 12 h | 24 h | 48 h |
| YGYS-L | 5% | 0.82 ±0.16 | 1.63 ±0.42* | 0.96 ±0.34 |
| | 10% | 0.78 ±0.12 | 1.24 ±0.26 | 1.10 ±0.51 |
| | 15% | 0.72 ±0.15 | 1.25 ±0.46 | 1.47 ±0.40 |
| | 20% | 0.56 ±0.09 | 1.25 ±0.31 | 1.23 ±0.25 |
| YGYS-M | 5% | 1.83 ±0.23* | 1.89 ±0.35*# | 1.58 ±0.11* |
| | 10% | 1.20 ±0.13 | 1.58 ±0.21* | 1.77 ±0.33* |
| | 15% | 0.97 ±0.07 | 1.81 ±0.47* | 1.28 ±0.29 |
| | 20% | 0.90 ±0.10 | 1.48 ±0.43 | 1.36 ±0.40 |
| YGYS-H | 5% | 0.89 ±0.06 | 1.34 ±0.69 | 1.46 ±0.38 |
| | 10% | 0.78 ±0.58 | 1.45 ±0.35 | 1.50 ±0.31 |
| | 15% | 0.72 ±0.05 | 1.33 ±0.23 | 1.71 ±0.66* |
| | 20% | 0.47 ±0.09 | 1.38 ±0.51 | 1.03 ±0.21 |

*Compared with control group, *p < 0.05; compared with YGYS-M 24 h – 20% group, #p < 0.05.*
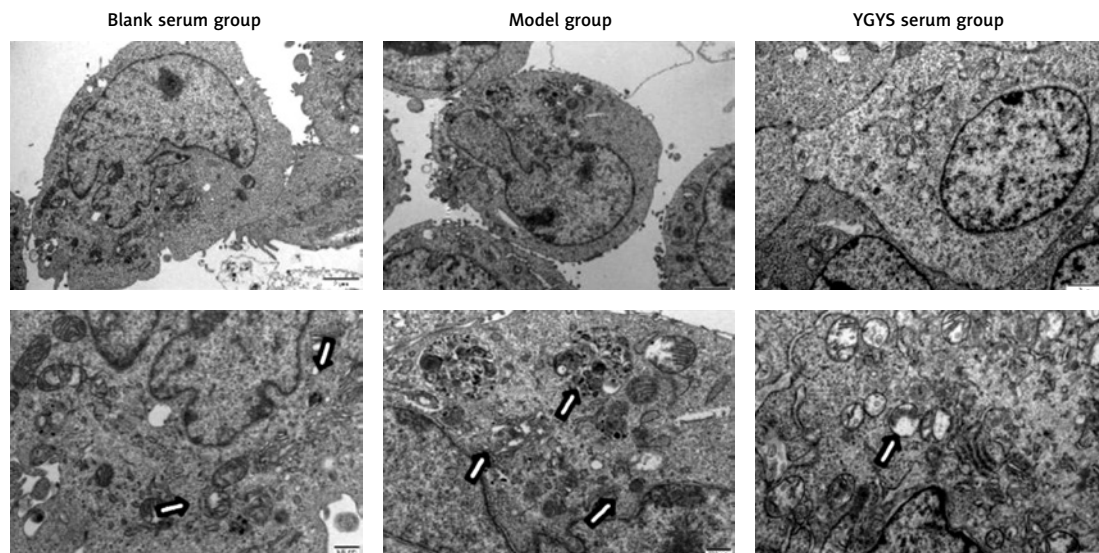


**Figure 9.** TEM of cells in each group

protein expression of LC3-II/LC3-I in the model, benazepril, YGYS-M, and YGYS-L groups was elevated ($p < 0.05$, Figures 10, 11). The expression of mTOR and p62 proteins in the model and YGYS-L groups was lower than that of the control group ($p < 0.05$, Figures 10, 11). Compared to the model group, the protein expression of PI3K, AKT, and beclin-1 in the 3-MA, benazepril, YGYS-H, and YGYS-M groups was downregulated ($p < 0.05$, Figures 10, 11), whereas the protein expression of mTOR in the 3-MA, benazepril, YGYS-H, and YGYS-M groups was upregulated ($p < 0.05$, Figures 10, 11). The protein expression of p62 in the 3-MA and YGYS-H groups was elevated, whereas that of LC3-II/LC3-I in the 3-MA and YGYS-H groups was decreased ($p < 0.05$, Figures 10, 11). Furthermore,

the expression of mTOR protein was downregulated in the benazepril, YGYS-H, and YGYS-M groups, whereas the expression of PI3K, AKT, beclin-1, and LC3-II/LC3-I in the YGYS-L group was higher ($p < 0.05$, Figures 10, 11) than that in the 3-MA group.

The RT-qPCR results showed that, compared to the control group, PI3K, AKT, and mTOR mRNA expression in the model, benazepril, YGYS-M, and YGYS-L groups was elevated ($p < 0.05$, Figure 12). Compared with the model group, PI3K, AKT, and mTOR mRNA expression in the 3-MA, benazepril, YGYS-H, YGYS-M, and YGYS-L groups was lower ($p < 0.05$, Figure 12). Compared to the 3-MA group, AKT and mTOR mRNA expression in the benazepril, YGYS-M, and YGYS-L groups was elevated ($p < 0.05$, Figure 12), and PI3K mRNA

expression in the YGYS-M and YGYS-L groups was elevated (*p* < 0.05, Figure 12). To clarify the relationship between YGYS-containing serum and autophagy, we conducted a response experiment. The results showed that the protein expression level of LC3-II/LC3-I in the YGYS-M + 3-MA (25 mM) group was significantly lower than that in the model group (*p* < 0.05, Figures 13, 14). Compared to the YGYS-M group, the protein expression level of LC3-II/LC3-I in the YGYS-M + 3-MA (25 mM) group was significantly lower (*p* < 0.05, Figures 13, 14). These results indicated that YGYSG and autophagy have a synergistic relationship in MPC-5 cells, and YGYSG may inhibit autophagic activity by activating the PI3K/AKT/mTOR signaling pathway.

## Discussion

Hypertension is a threat to global human health, and its incidence is increasing annually [30]. Chronic uncontrolled hypertension can also lead to kidney damage [31]. Traditional Chinese medicine, which has multiple targets and fewer side effects, plays an important role in the treatment of hypertension. Previous studies have shown that YGYSG improves vascular endothelial disorders, regulates blood pressure and inflammatory responses, and improves clinical symptoms in patients with HRD [32].

Autophagy is the process of self-degradation of damaged organelles to maintain homeostasis in the intracellular environment [33]. Autophagy has long been considered beneficial to the body because it can help remove harmful pathogen products and simultaneously degrade discarded organelles to produce nutrition energy [34, 35]. This is most evident in the early development of tumors [36]. However, autophagy is a double-edged sword and abnormally activated autophagy can cause cell damage [37]. Recent studies have shown that autophagy is involved in kidney disease and is closely related to HRD. Long-term hypertension leads to abnormal renal autophagy, an important factor in HRD progression and development [27]. In this study, the associated targets and signaling pathways of YGYSG, autophagy, and HRD were screened using network pharmacology. Network pharmacological analysis showed that the core components of YGYS used to treat hypertensive kidney injury through the autophagy pathway were quercetin, kaempferol, beta-sitosterol, stigmasterol, luteolin, isorhamnetin, tanshinone II, 7-O-methylisomucronulatol, baicalein, and formononetin. Studies have found that quercetin has physiological effects on cell apoptosis, autophagy, pyroptosis, and other cellular processes [27] and inhibits the formation
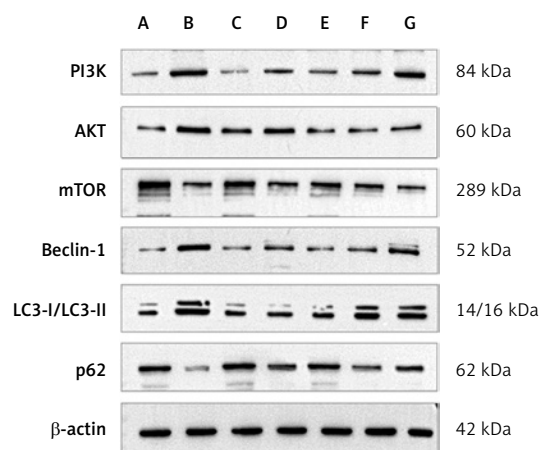


**Figure 10.** Protein expression of PI3K, AKT, mTOR, beclin-1, LC3-II/LC3-I, p62 in each group. A – Control group; B – Model group; C – 3-MA group; D – Benazepril group; E – YGYS-H group; F – YGYS-M group; G – YGYS-L group. Compared with control group, *\**p* < 0.05; compared with model group, #*p* < 0.05; compared with 3-MA groups, Δ*p* < 0.05

of kidney autophagosomes in mice by inhibiting oxidative stress [36]. Kaempferol can regulate beclin-1, LC3, and endoplasmic reticulum stress levels [38] and inhibit the autophagic activity of cells by degrading p62/SQSTM1 [39]. Luteolin can reduce Ang II-induced kidney injury in HRD [40] and regulate autophagy in kidney injury by participating in the AMPK/mTOR signaling pathway [41]. As a flavonoid, isorhamnetin is involved in the treatment of liver, tumors, and other diseases [42] and plays various inhibitory roles in autophagy [43]. This suggests that our bioinformatics analysis is consistent with existing reports, indicating that YGYSG may alleviate HR by regulating cellular autophagy.

Ang II is an important activator of the RAAS system, which plays an important role in the pathogenesis of HRD and renal autophagy. Studies have found that in patients with HRD, the concentration of Ang II in the kidney is higher than that in circulating blood [44], and Ang II can directly act on podocytes, resulting in excessive autophagy [45]; therefore, we chose Ang II for *in vitro* stimulation. Excessive autophagy induced by Ang II aggravates damage to the renal blood vessels and podocytes [27]. Our previous studies showed that YGYSG regulates Ang II levels during HRD treatment [46]. TEM observations showed that Ang II-stimulated podocytes showed over-expanded autophagosomes, the number of which increased greatly, and the structure of the organelles was destroyed, as has been reported by previous authors. Notably, the number and morphology of autophagosomes in the YGYSG group were normal and the morphology of the organelles was improved. The core targets identified by the protein interaction analy-
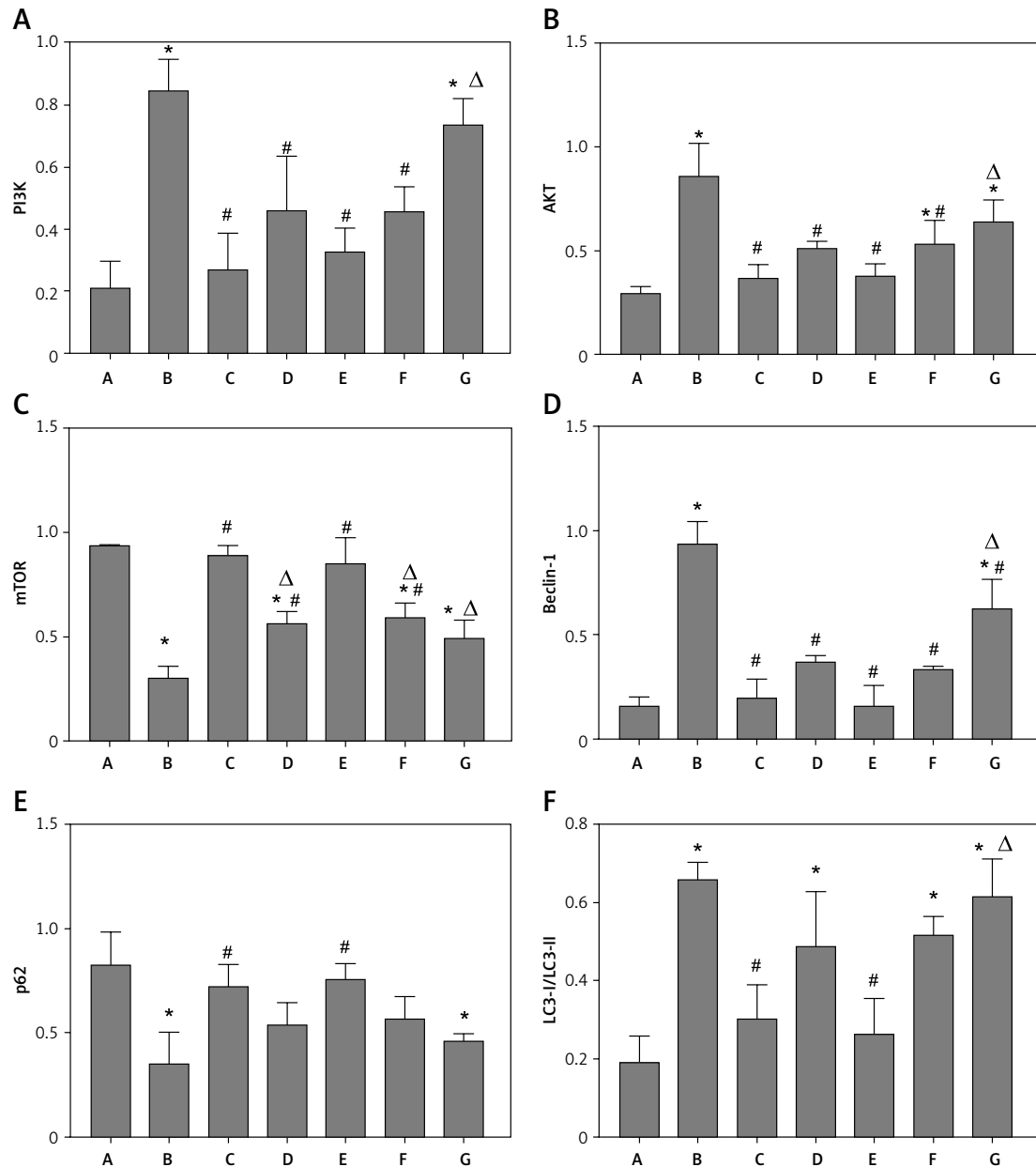
**Figure 11.** Quantitative analysis of protein expression of PI3K (**A**), AKT (**B**), mTOR (**C**), beclin-1 (**D**), p62 (**E**), and LC3-I/LC3-II (**F**), in each group. A – Control group; B – Model group; C – 3-MA group; D – Benazepril group; E – YGYS-H group; F – YGYS-M group; G – YGYS-L group. Compared with control group, *$p < 0.05$; compared with model group, #$p < 0.05$; compared with 3-MA groups, Δ$p < 0.05$

sis were TP53, AKT1, STAT3, JUN, CASP3, TNF, MYC, MTOR, EGFR, and MAPK1. Most of these targets are associated with inflammation and REDOX. In the state of hypertension, inflammatory products accumulate in renal vessels, and the protein expression of AKT1, STAT3, and TNF, which are important markers of hypertensive kidney injury, is upregulated [47].

Furthermore, we demonstrated that the HRD targets of YGYSG were mainly enriched in the PI3K/AKT/mTOR signaling pathway and mTOR signaling; therefore, we selected the PI3K/AKT/mTOR signaling pathway as the focus of further

research. PI3K, a phosphatidylinositol kinase, activates the downstream target growth factor receptor (EGFR), which alters AKT protein structure. The mammalian target proteins of rapamycin (mTOR) are divided into mTOR1 and mTOR2, with mTOR1 being a key target in the regulation of autophagy [48]. When the intracellular energy levels are unbalanced, PI3K/AKT and mTOR are activated, inhibiting autophagy [6]. Compared to the model group, the protein expression of PI3K, AKT, beclin-1, and LC3-II/LC3-I was downregulated after YGYSG treatment, whereas the protein expression of mTOR and p62 was upregulated. These results
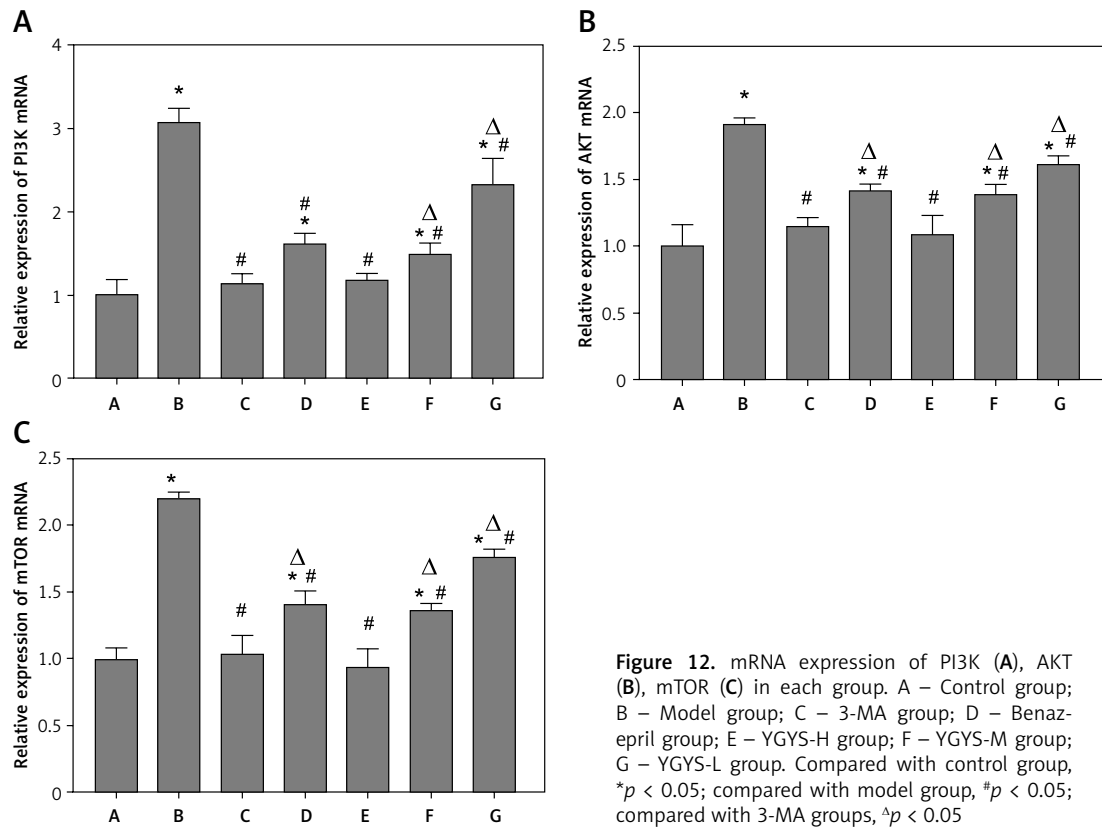
**A**



**B**



**C**



**Figure 12.** mRNA expression of PI3K (**A**), AKT (**B**), mTOR (**C**) in each group. A – Control group; B – Model group; C – 3-MA group; D – Benazepril group; E – YGYS-H group; F – YGYS-M group; G – YGYS-L group. Compared with control group, *$p < 0.05$; compared with model group, #$p < 0.05$; compared with 3-MA groups, △$p < 0.05$
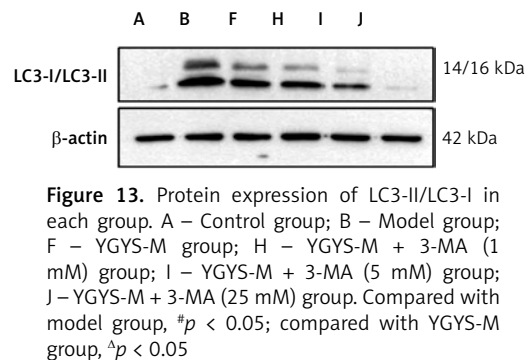


**Figure 13.** Protein expression of LC3-II/LC3-I in each group. A – Control group; B – Model group; F – YGYS-M group; H – YGYS-M + 3-MA (1 mM) group; I – YGYS-M + 3-MA (5 mM) group; J – YGYS-M + 3-MA (25 mM) group. Compared with model group, #$p < 0.05$; compared with YGYS-M group, △$p < 0.05$
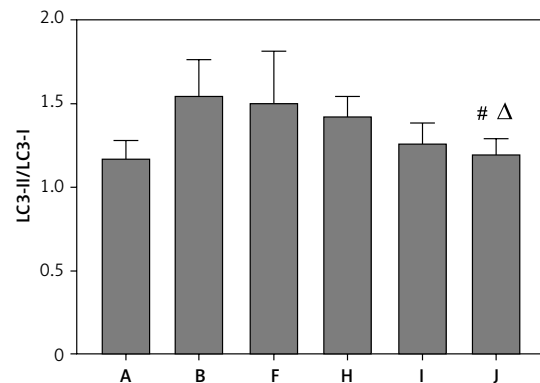


**Figure 14.** Quantitative analysis of protein expression of LC3-II/LC3-I in each group. A – Control group; B – Model group; F – YGYS-M group; H – YGYS-M + 3-MA (1 mM) group; I – YGYS-M + 3-MA (5 mM) group; J – YGYS-M + 3-MA (25 mM) group. Compared with model group, #$p < 0.05$; compared with YGYS-M group, △$p < 0.05$

are consistent with previous reports, indicating that YGYSG may alleviate HRD by regulating the PI3K/AKT/mTOR signaling pathway and modulating autophagy processes.

Certainly, this study has some limitations. In the cell experiment, we conducted a small response experiment to show the relationship between YGYSG and autophagy. However, the mechanism of action of YGYSG for Ang II-induced hyperautophagy in renal podocytes requires further investigation. In the future, we will verify the effect of YGYSG on the regulation of HRD through the PI3K/AKT/mTOR pathway *in vivo* and conduct further *in vitro* experiments to provide a possible basis for the treatment of HRD using traditional Chinese medicine.

In conclusion, our results showed a synergistic relationship between YGYSG and autophagy in HRD. This study utilized network pharmacol-

ogy and *in vitro* experiments to investigate the effects of YGYSG on HRD through the autophagy pathway. Network pharmacology identified key targets and compounds associated with YGYSG's action, focusing on the PI3K/AKT/mTOR signaling pathway and autophagy-related processes. *In vitro* experiments using Ang II-stimulated renal podocytes demonstrated that YGYSG exerts therapeutic effects by modulating autophagy via the PI3K/AKT/mTOR pathway in hypertensive renal damage. This study has important implications for

Pan Liu, Tairan Hu, Bing Gao, Ran Xia, Xiaohua Dai, Jing Wang

improving outcomes in HRD research and clinical practice.

## Acknowledgments

## Data availability statement

The original contributions proposed in the study are included in the article/supplementary materials, and further inquiries can be directly addressed to the corresponding author.

## Funding

## Ethical approval

This study was approved by the Experimental Animal Ethics Committee of Anhui University of Traditional Chinese Medicine (AHUCM-rats-2021135).

## Conflict of interest

The authors declare no conflict of interest.

## References

1. Wierzejska E, Giernaś B, Lipiak A, Karasiewicz M, Cofta M, Taszewski R. A global perspective on the costs of hypertension: a systematic review. Arch Med Sci 2020; 16: 1078-91.
2. Burnier M, Damianaki A. Hypertension as cardiovascular risk factor in chronic kidney disease. Circ Res 2023; 132: 1050-63.
3. Forouzanfar MH, Liu P, Roth GA, et al. Global burden of hypertension and systolic blood pressure of at least 110 to 115 mm Hg, 1990–2015. JAMA 2017; 317: 165-82.
4. Hart PD, Bakris GL. Hypertensive nephropathy: prevention and treatment recommendations. Expert Opin Pharmacother 2010; 11: 2675-86.
5. Yan SH, Zhao NW, et al. Hsp90beta is involved in the development of high salt-diet-induced nephropathy via interaction with various signalling proteins. Open Biol J 2016; 6: 150159.
6. Ma L, Zhang R, Li D, Qiao T, Guo X. Fluoride regulates chondrocyte proliferation and autophagy via PI3K/AKT/mTOR signaling pathway. Chem Biol Interact 2021; 349: 109659.
7. Lu X, Crowley SD. Inflammation in salt-sensitive hypertension and renal damage. Curr Hypertens Rep 2018; 20: 103.
8. Agita A, Alsagaff MT. Inflammation, immunity, and hypertension. Acta Med Indones 2017; 49: 158-65.
9. Chinese Society of Cardiology, Chinese Medical Association, Editorial Board of Chinese Journal of Cardiology. Chinese experts consensus on diagnosis and management of salt-sensitive hypertension. Zhonghua Xin Xue Guan Bing Za Zhi 2023; 51: 364-76.
10. Lee KJ, Ryu JK, Cho YH, et al. Effectiveness and safety of a fixed-dose combination of valsartan and rosuvastatin (Rovatitan® tablet) in patients with concomitant hypertension and hyperlipidemia: an observational study. Drug Des Dev Ther 2023; 17: 1047-62.
11. Zhao Q, Li Y, Chen C. Current status and prospects of research on mechanism of action of traditional Chinese medicine in treating essential hypertension. Chin J 2020; 35: 1914-6.
12. Huang K, Zhang P, Zhang Z, et al. Traditional Chinese Medicine (TCM) in the treatment of COVID-19 and other viral infections: efficacies and mechanisms. Pharmacol Ther 2021; 225: 107843.
13. Li S, Wu Z, Le W. Traditional Chinese medicine for dementia. Alzheimers Dement 2021; 17: 1066-71.
14. Weiping LI, Yunhai Z, Junhua W, et al. Treatment effect of Yanggan Yishui granule on early renal injury in hypertension patients and the effect on blood pressure variability. Chin Arch Trad Chin Med 2018; 36: 1917-9.
15. Dai Xh, Xu ZJ, Qi XW, et al. The effects of Yanggan-Yishui granules on early renal damage in hypertension and multiple cardiovascular risk factors. J Cardiovasc Cerebrovasc Dis Integr Tradit Chin West Med 2017; 015: 901-4.
16. Gu JX. Observing the effects of Zhou's Yanggan-Yishui granules on alleviating early renal damage in primary hypertension. J Clin Tradit Chin Med 2005; 17: 373-4.
17. Shen DQ, Dai XH, Yang F, et al. Effects of Yanggan-Yishui granules on the AngII/TRPC6/NF-κB pathway in rats with early hypertensive renal damage. N Drugs Tradit Chin Med Clin Pharmacol 2022; 033.
18. Cai MM, Long ZJ, Zhou YH, Ding BC, Chen C, Lu SX. Effects of Yanggan Yishui granules on renal TGF-β1, PI3K, and PKB in spontaneously hypertensive rats. Drug Evaluation Study 2013; 4.
19. Chen J, Yuan S, Zhou J, et al. Danshen injection induces autophagy in podocytes to alleviate nephrotic syndrome via the PI3K/AKT/mTOR pathway. Phytomedicine 2022; 107: 154477.
20. Yang Y, Hong M, Lian WW, Chen Z. Review of the pharmacological effects of astragaloside IV and its autophagic mechanism in association with inflammation. World J Clin Cases 2022; 10: 10004-16.
21. Teh YM, Mualif SA, Lim SK. A comprehensive insight into autophagy and its potential signaling pathways as a therapeutic target in podocyte injury. Int J Biochem Cell Biol 2022; 143: 106153.
22. Ding K, Wang Y, Jiang W, Zhang Y, Yin H, Fang Z. Qian Yang yu yin granule- containing serum inhibits angiotensin II-induced proliferation, reactive oxygen species production, and inflammation in human mesangial cells via an NADPH oxidase 4-dependent pathway. BMC Complement Altern Med 2015; 15: 81.
23. Dong Q, Xing W, Fu F, et al. Tetrahydroxystilbene glucoside inhibits excessive autophagy and improves microvascular endothelial dysfunction in prehypertensive spontaneously hypertensive rats. Am J Chin Med 2016; 44: 1393-412.
24. Dryer SE, Reiser J. Trpc6 channels and their binding partners in podocytes: role in glomerular filtration and

pathophysiology. Am J Physiol Ren Physiol 2010; 299: F689-701.

25. Seong SB, Ha DS, Min SY, Ha TS. Autophagy precedes apoptosis in angiotensin II-induced podocyte injury. Cell Physiol Biochem 2019; 53: 747-59.

26. van Kats JP, Schalekamp MA, Verdouw PD, Duncker DJ, Danser AH. Intrarenal angiotensin II: interstitial and cellular levels and site of production. Kidney Int 2001; 60: 2311-7.

27. Yadav A, Vallabu S, Arora S, et al. Ang II promotes autophagy in podocytes. Am J Physiol Cell Physiol 2010; 299: C488-96.

28. Ru JL, Li P, Wang JA, et al. TCMSP: a database ofsystems pharmacology for drug discovery from herbal medicines. J Cheminform 2014; 6: 13.

29. Hou FF, Yu ZY, Cheng Y, Liu Y, Liang S, Zhang F. Deciphering the pharmacological mechanisms of Scutellaria baicalensis Georgi on oral leukoplakia by combining network pharmacology, molecular docking and experimental evaluations. Phytomedicine 2022; 103: 154195.

30. Guwatudde D, Nankya-Mutyoba J, Kalyesubula R, et al. The burden of hypertension in sub-Saharan Africa: a four-country cross sectional study. BMC Publ Health 2015; 15: 1211.

31. Sun D, Wang JJ, Wang W, et al. Human podocyte injury in the early course of hypertensive renal injury. World J Clin Cases 2019; 7: 3698-710.

32. Yexiang Z, Xiaoyu C, Yebin HU, et al. Effect of Yanggan Yishui granule on blood pressure variability, vascular endothelial function and urinary protein in patients with hypertension of yin deficiency Yang hyperactivity type/ ZHANG Beibei. Chin Med Innov 2021; 18: 95-9.

33. Zuo H, Chen C, Sa Y. Therapeutic potential of autophagy in immunity and inflammation: current and future perspectives. Pharmacol Rep 2023; 75: 499-510.

34. Oyagbemi AA, Omobowale TO, Ola-Davies OE, et al. Quercetin attenuates hypertension induced by sodium fluoride via reduction in oxidative stress and modulation of HSP 70/ERK/PPARγ signaling pathways. BioFactors 2018; 44: 465-79.

35. Zhang P, Liao J, Wang X, Feng Z. High glucose promotes apoptosis and autophagy of MC3T3-E1 osteoblasts. Arch Med Sci 2023; 19: 138-50.

36. Yuan Y, Ma S, Qi Y, et al. Quercetin inhibited cadmium-induced autophagy in the mouse kidney via inhibition of oxidative stress. J Toxicol Pathol 2016; 29: 247-52.

37. Chen L, Zhang B, Toborek M. Autophagy is involved in nanoalumina-induced cerebrovascular toxicity. Nanomed Nanotechnol Biol Med 2013; 9: 212-21.

38. Ashrafizadeh M, Tavakol S, Ahmadi Z, Roomiani S, Mohammadinejad R, Samarghandian S. Therapeutic effects of kaempferol affecting autophagy and endoplasmic reticulum stress. Phytother Res 2020; 34: 911-23.

39. Kim CJ, Shin SH, Kim BJ, et al. The effects of kaempferol-inhibited autophagy on osteoclast formation. Int J Mol Sci 2018; 19: 125.

40. Liu YS, Yang Q, Li S, et al. Luteolin attenuates angiotensin II-induced renal damage in apolipoprotein E-deficient mice. Mol Med Rep 2021; 23: 157.

41. Xu X, Yu Z, Han B, et al. Luteolin alleviates inorganic mercury-induced kidney injury via activation of the AMPK/ mTOR autophagy pathway. J Inorg Biochem 2021; 224: 111583.

42. Liu N, Feng J, Lu X, et al. Isorhamnetin inhibits liver fibrosis by reducing autophagy and inhibiting extracellular matrix formation via the TGF-β1/Smad3 and TGF-β1/ p38 MAPK pathways. Mediators Inflamm. 2019; 2019: 6175091.

43. Lu X, Liu T, Chen K, et al. Isorhamnetin: a hepatoprotective flavonoid inhibits apoptosis and autophagy via P38/PPAR-α pathway in mice. Biomed Pharmacother 2018; 103: 800-11.

44. Nishiyama A, Kobori H. Independent regulation of renin-angiotensin- aldosterone system in the kidney. Clin Exp Nephrol 2018; 22: 1231-9.

45. Lara LS, McCormack M, Semprum-Prieto LC, et al. At1 receptor-mediated augmentation of angiotensinogen, oxidative stress, and inflammation in ang II-salt hypertension. Am J Physiol Ren Physiol 2012; 302: F85-94.

46. Xiaohua D, Yi J. Effect of Yanggan Yishui granules on plasma Ang II, AT1R content and renal, AT1R, TRPC6 protein expression in spontaneous hypertensive rats. Lishizhen Med Materia Med Res 2021; 32: 1877-80.

47. Mennuni S, Rubattu S, Pierelli G, Tocci G, Fofi C, Volpe M. Hypertension and kidneys: unraveling complex molecular mechanisms underlying hypertensive renal damage. J Hum Hypertens 2014; 28: 74-9.

48. Dou F, Liu Y, Liu L, et al. Aloe-emodin ameliorates renal fibrosis via inhibiting PI3K/Akt/mTOR signaling pathway in vivo and in vitro. Rejuvenation Res 2019; 22: 218-29.